Convection in TOGA COARE: Horizontal Scale, Morphology, and Rainfall Production

THOMAS M. RICKENBACH* AND STEVEN A. RUTLEDGE

Department of Atmospheric Science, Colorado State University, Fort Collins, Colorado

(Manuscript received 30 August 1996, in final form 5 December 1997)

ABSTRACT

The occurrence frequency and rainfall production of mesoscale convective systems (MCSs) relative to smaller groups of convective clouds over the tropical oceans is not well known. Eighty days of shipboard radar data collected during the recent Tropical Ocean Global Atmosphere Coupled Ocean–Atmosphere Response Experiment (TOGA COARE) were used to provide a detailed view of convection in the western Pacific warm pool, a region of global climatological significance. The aim of this study was to document the frequency of occurrence, rainfall production, and depth of convection observed during TOGA COARE within a simple and meaningful framework of convective horizontal organization. Organization was characterized in terms of the horizontal scale and morphology of convective systems. Precipitation events were defined based on whether they attained the length scale of an MCS, and on whether convection was organized into lines.

About four-fifths of rainfall during COARE was associated with MCS-scale squall lines. These occurred in a variety of wind regimes but tended to be most common prior to low-level westerly wind maxima. Systems of isolated cells produced 12% of all COARE rainfall and were observed during periods of both very weak and very strong low-level winds. These two modes occurred about equally as often, and together they accounted for about 90% of observed convection. Cloud height populations associated with MCS organization were distinct from sub-MCS-scale cloud systems, with more rainfall from shallower clouds for sub-MCS convection. The distribution of total rainfall by cloud height for COARE was interpreted as a superposition of rainfall-cloud height distributions from each mode of organization. These results raise the possibility that isolated cell periods may represent a distinct, nonnegligible heat source in the large-scale heat budget when compared to the dominant MCS-scale systems.

1. Introduction

Precipitating cumulus convection in the Tropics is manifested over a large range of spatial scales. Individual convective cells occur on the micro-α scale (several hundred meters to a few kilometers; Orlanski 1975), whereas the merged anvils of mesoscale regions of precipitation can form meso-α scale super cloud clusters several thousand kilometers in length (Nakazawa 1988). On the meso-β scale (20–200 km), a common mode of convective organization is the mesoscale convective system (MCS). An MCS is defined as a group of thunderstorms with a contiguous precipitation region of at least 100 km (this length scale is herein referred to as the ''MCS scale''), often with an extensive precipitating anvil cloud, which can reach several hundred kilometers in horizontal extent (Cotton and Anthes 1991; Houze 1993). MCSs have been shown to contain both regions of convective cells and stratiform rain. These regions are linked dynamically and microphysically through momentum and condensate transport by mesoscale flow features and through energy transport by gravity waves (Leary and Houze 1979; Zipser et al. 1981; LeMone 1983; Churchill and Houze 1984; Rutledge and Houze 1987; Schmidt and Cotton 1989; Biggerstaff and Houze 1991).

Previous studies of convection on the meso-β scale have focused on the importance of the scale and morphology of convective organization to the vertical structure of heat and momentum transport. Riehl and Malkus (1958) hypothesized that vertical energy transport occurs on the scale of the convective cell, in the undilute cores of convective ''hot towers.'' More recently, Houze (1982) suggested that the effect of convection on large-scale circulations may be viewed with the mesoscale convective system (MCS) as the fundamental unit of vertical energy transport.

Within MCSs, heat and momentum transports differ greatly between convective and stratiform components of the system (Zipser 1977; Houze 1989). LeMone (1983) concluded that the momentum flux in a tropical squall line system was initiated in the convective region

* Current affiliation: National Research Council Research Associate, Tropical Rainfall Measuring Mission Office, NASA Goddard Space Flight Center, Greenbelt, Maryland.

Corresponding author address: Prof. Steven A. Rutledge, Dept. of Atmospheric Science, Colorado State University, Ft. Collins, CO, 80523.
E-mail: rutledge@olympic.atmos.colostate.edu.

at the leading edge of the line, with little contribution from the trailing stratiform region. Similarly, the vertical distribution of heating is distinct for the convective and stratiform components of an MCS. Heating in the convective region is strongest at lower levels, whereas upper-level heating and lower-level cooling characterizes the anvil region (Houze 1982; Johnson 1984).

In terms of morphology, the organization of convection into lines influences the vertical momentum transports. The system-relative ascending front-to-rear and descending rear-to-front flow features associated with many organized squall lines tend to increase momentum at upper levels against the line propagation direction and increase momentum at low levels in the direction of line propagation (LeMone et al. 1984). Convection without linear organization does not show consistent momentum transport properties (LeMone et al. 1984).

Many previous studies have classified the convective organization of radar echoes to understand the observed variability in the horizontal precipitation morphology of MCSs. Each of these studies developed distinct classification schemes designed to study specific hypotheses and reflect recurrent trends in the data. Accordingly, differences in the bases of classification reflected both what the investigator viewed as the important attributes, which characterized the range of structural variability, and the system properties under investigation.

In a summary of GARP (Global Atmospheric Research Program) Atlantic Tropical Experiment (GATE) observational studies, Houze and Betts (1981) characterized convection in the tropical eastern Atlantic Ocean as being associated with squall clusters and nonsquall clusters, delineated by differences in propagation speed and downdraft intensity. These differences were attributed to the strength of the vertical wind shear. Bluestein and Jain (1985) studied the formation of lines of convective cells in the southern plains of the United States. They developed a four category classification to study the horizontal pattern of precipitation associated with the formative stage of convective lines, determined from radar reflectivity data. They characterized each category in terms of the convective available potential energy and vertical wind shear of the formation environment. Using satellite and radar data from the Amazon Boundary Layer Experiment in the Amazon Basin, Greco et al. (1990) adopted a different approach, classifying convection by region of origin relative to significant topography or proximity to coastal areas affected by the land–sea-breeze circulation. They discussed differences in morphology and propagation in terms of convective initiation mechanisms specific to each region. Houze et al. (1990) examined the morphological characteristics of the significant rain-producing systems during three spring seasons in Oklahoma. They described systems in terms of their degree of conformity to an idealized squall line with a broad region of trailing stratiform rain, as well as to what degree systems contained a spatially symmetric leading convective line and trailing stratiform region. Keenan and Carbone (1992) studied differences in break versus monsoon convection in the vicinity of Darwin, Australia. They categorized convective systems based on the dominant flow regime within which each system formed, discussing similarities and differences in oceanic monsoon systems (northwest flow from the ocean) and continental ''break period'' systems (southeast flow from the continent). More recently, Loehrer and Johnson (1995) examined the morphology of convective systems in the central plains of the United States in the context of the symmetric versus asymmetric structure classification discussed by Houze et al. (1990). They concluded that these two organizational modes were not distinct system types, but represented different stages in the life cycle of a general class of squall line MCSs.

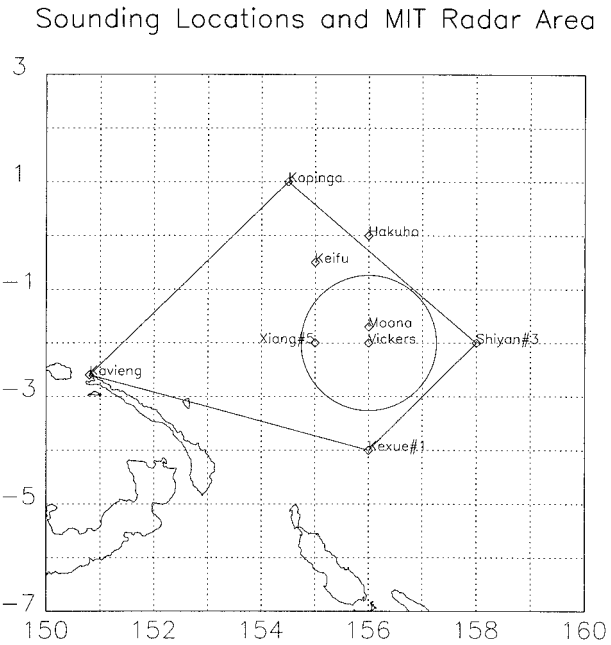

FIG. 1. Location of the MIT radar study area (circle of 120-km radius) and soundings used to estimate the zonal wind profile near the radar.

The recent Tropical Ocean Global Atmosphere Coupled Ocean–Atmosphere Response Experiment (TOGA COARE; Webster and Lukas 1992) resulted in a detailed view of tropical oceanic convection in the western Pacific warm pool region. The shipboard radar component of COARE provided a nearly continuous three-month Eulerian meso-β-scale sample of the precipitation structure of tropical oceanic convection. The strength of this dataset was that it allowed a systematic comparison of all observed convection, from unorganized isolated cells to large mesoscale systems. The aim of this study was to document the occurrence, rainfall production, and depth of convection observed during TOGA COARE within a simple and meaningful framework of convective horizontal organization. This organization was ex-

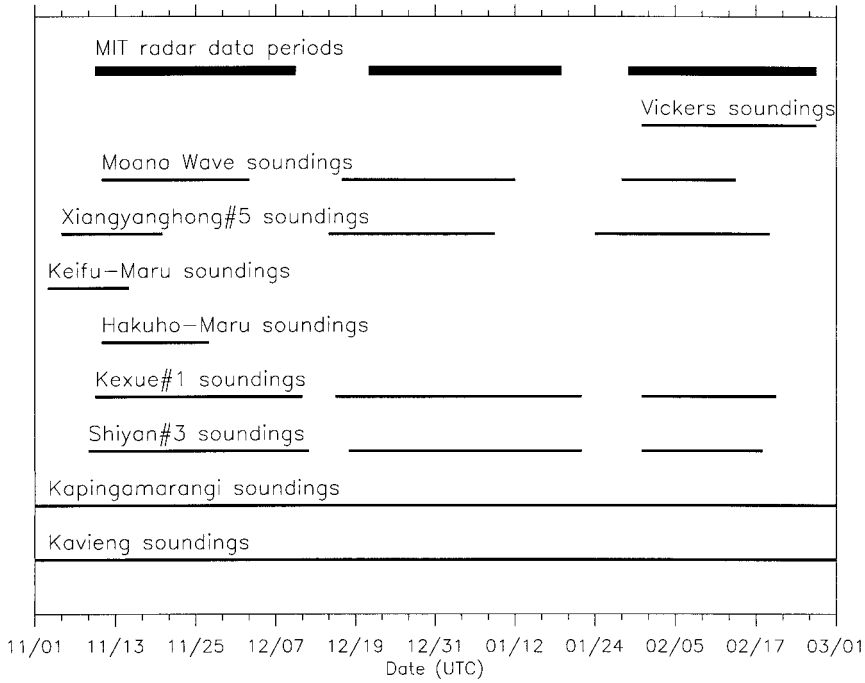

FIG. 2. Time periods of data collection of the MIT radar and each sounding station used in this study. Time interval of each tick mark is four days.

amined in the context of the horizontal scale (sub-MCS vs MCS scale) and morphology (linear vs nonlinear organization) of convective precipitation features. The frequency of occurrence, rainfall production, and depth of convection was then diagnosed within this context. These results were examined in relation to the time-varying large-scale features of the zonal wind in the vicinity of the radar observations. This study represents a climatological perspective on mesoscale convective organization for the warm pool region, which provides a context in which to place detailed studies of individual convective events.

The paper is organized as follows: the radar reflectivity and sounding data are described in section 2, the classification of organization, convective–stratiform partitioning, and the definition of convective features are given in section 3, and in section 4 rainfall and occurrence frequency statistics and distributions of convective features by height for each mode of organization are presented. Results are summarized in section 5.

2. Data

Radar reflectivity data were collected with the Massachusetts Institute of Technology (MIT) C-band Doppler radar, deployed aboard the R/V *Vickers* (Rutledge et al. 1993), and by the National Aeronautics and Space Administration TOGA C-band Doppler radar mounted on the Chinese research vessel *Xiangyanghong #5* (Short et al. 1997). Because of the large amount of data processing involved in analyzing the three-dimensional reflectivity values, only the MIT radar data was used for this study. The radar operated during three cruises of the *Vickers*, between November 1992 and February 1993, as part of the COARE intensive observation period (IOP). For each cruise, the ship maintained a nearly fixed position at approximately 2°S, 156°E, with a one-week interruption in data collection between cruises. Data was collected almost continuously while the ship was on station, for a total of about 80 days.

Reflectivity volume scans were analyzed at 20-min intervals for the 80 days of data collection, or just over 6000 volumes. The reflectivity data were interpolated from polar to Cartesian coordinates to a 2-km horizontal, 0.5-km vertical grid. The grid origin was fixed in space at the nominal position of the ship to correct the echo locations for ship motion. Only reflectivity data within 120 km of the radar were used for rainfall calculations, since beam broadening beyond this range smoothed convective cell spatial structures in the reflectivity field below acceptable limits. All subsequent analysis was performed at a constant altitude of 2 km MSL. This value was chosen as a compromise between the need to produce rainfall estimates close to the surface and the increase in horizontal reflectivity data coverage with height. At times of strong surface wind speed, scattering of the radar beam off the crests of large ocean waves sometimes produced weak reflectivities near the surface around the radar (sea clutter). For these periods (about 3% of the data), the horizontal reflectivity pattern was

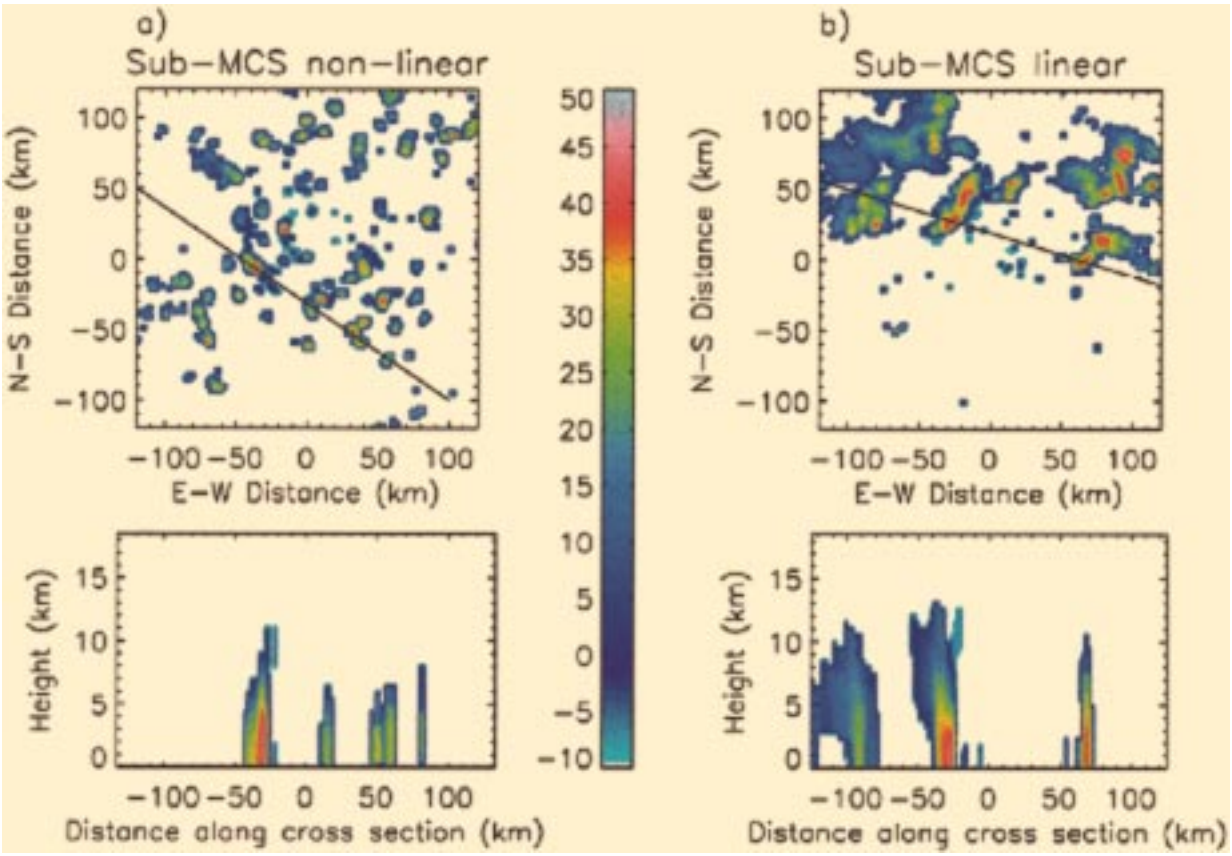

FIG. 3. Maps of radar reflectivity (dBZ) at a height of 2 km (upper panel) and vertical cross section of reflectivity (lower panel) for (a) a sub-MCS nonlinear event at 0721 UTC 2 December 1992, (b) a sub-MCS linear event at 1002 UTC 27 December 1992. (c) an MCS nonlinear event at 1802 UTC 15 January 1993, and (d) an MCS linear event at 0331 UTC 25 December 1992. The solid black line on the horizontal map shows the location of the vertical cross section. The vertical cross section follows the solid black line from west to east.

analyzed at 3 km, which removed most of the clutter. Finally, all reflectivity values were increased by 2.4 dBZ to account for a correction to the antenna gain, and for a missing bandwidth term in the radar equation. Details of the rainfall estimation procedure from the reflectivity values are presented in section 3.

Radiosonde data within the intensive flux array (IFA) were used to characterize the mean state of the zonal wind in the vicinity of the radar. These data were used to place the radar observations into a general large-scale context (e.g., occurrence of westerly wind bursts or weak wind periods). The sounding data were taken from the six-hourly gridded analysis of Lin and Johnson (1996a) at a point representative of the nominal location of the MIT radar (R/V *Vickers*) near the center of the IFA (2°S, 156°E). The location of the sounding sites and the MIT radar sampling area is shown in Fig. 1. The vertical profile of the wind at that point was estimated by a Barnes objective analysis of the nearest soundings. The influence of each sounding was weighted linearly with distance from the radar. Shown in Fig. 2 are the periods of data availability of the MIT radar and each sounding site.

3. Analysis methods

a. Rainfall events: Scale and morphology

During COARE a broad spectrum of convective organization spatial scale and morphology was observed by shipboard radar. The variety, complexity, and persistence of COARE convection presented a challenge to not only account for this diversity, but to interpret it in terms of the limited spatial sample provided by a stationary platform. The spatial scale of the sample area (240 km × 240 km) was large enough to observe all or a significant portion of an MCS. On the other hand, the areal coverage of the radar limited the temporal sample to the time required for systems to propagate across the sample area (typically 6–12 h). The goals of this study and analysis techniques were intimately tied to these sampling considerations.

The two general goals of the present classification were to distinguish between convection, which organized to attain the length scale of an MCS (>100 km) from that which did not, and to distinguish between convection, which attained linear organization from that which did not, resulting in a four category classification.

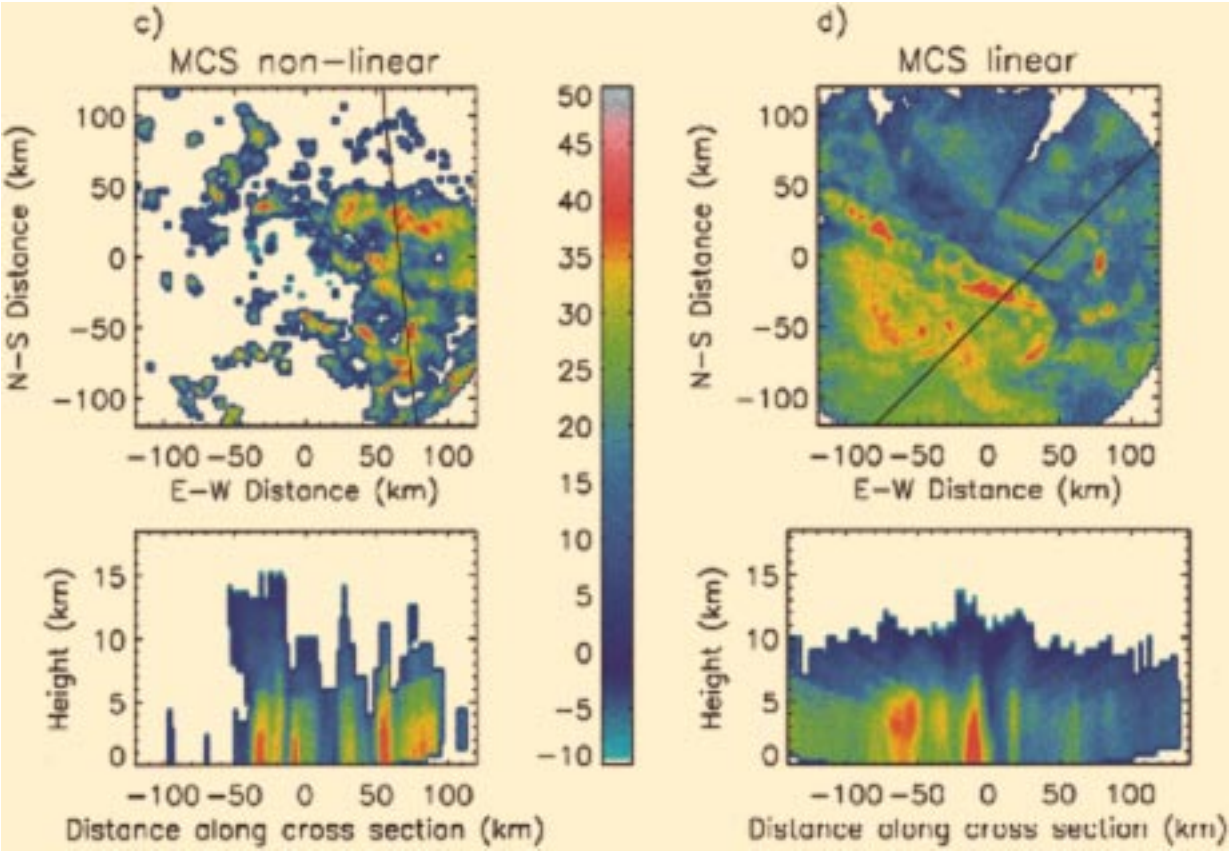

FIG. 3. (*Continued*)

The hierarchy of organization (implied by terms like ''less'' or ''lower'' and ''more'' or ''higher'') defined in this scheme was first nonlinear versus linear within the sub-MCS scale, then nonlinear versus linear within the MCS scale. The approach was to divide the entire dataset in time into contiguous ''events,'' with the convective organization of each event characterized by one of the four categories, as described below. An event is defined generally as convection occurring within a time period during which the largest group of convective cells maintained a particular mode of organization (this definition is developed further later in this section). The assessment of scale and morphology of each event was performed manually by examining horizontal reflectivity maps and tracking the size and structure of groups of convective cells. To be called a ''line,'' a cell group was required to have an aspect ratio of at least 5:1 (Bluestein and Jain 1985).

The simplest mode of organization was called ''sub-MCS nonlinear,'' which corresponded to a field of randomly spaced or small groups of isolated cells. An example of the horizontal reflectivity pattern and a vertical cross section during a sub-MCS nonlinear event is shown in Fig. 3a. This mode was considered to be the background or ''default'' mode, when none of the higher organization levels were present. The transition to a new event was defined to occur when more organized convection either formed within or entered into the radar view, provided that the new convection persisted for at least 1 h. At this stage, the new event was classified by the highest sustained (at least 1 h) level of organization attained by the new convection. The assignment of a class of organization was limited to the time period during which the convection remained within the radar domain (generally at least 6 h). This requirement prevented transient features not associated with the general organization of the event from influencing the characterization of organization. This also accounted for the evolution of an event, assigning the category that described the event's morphology at the highest level of organization. For example, this ensured that stratiform echo associated with a squall line, which had decayed or left the radar domain, remained as part of the squall line event.

When convection developed linear organization no greater than 100 km in length without transitioning to another event, the event was termed ''sub-MCS linear.'' A lower length scale limit of 50 km was used by Bluestein and Jain (1985) as the smallest length scale of a convective line; therefore, lines of convection were required to be at least 50 km in length to distinguish linear from nonlinear organization. Sub-MCS linear systems

generally consisted of the convective cells, which formed the line with small regions of stratiform precipitation forming upon decay of the convection (the presence of stratiform echo was not tied to the definition of any event type). An example is given in Fig. 3b, which shows several small lines of convection on 27 December 1992. Several lines of convection generally appeared together within a particular sub-MCS linear event.

Alternately, when convection developed into a random amalgam of convective cells of more than 100 km in length, with no persistent linear organization, the event was called ''MCS nonlinear.'' These events were characterized by a large convective region comprising convective cells organized into a random, clustered pattern. These events generally formed from the merger of isolated cells and groups of cells, which connected to form a single broad convective region. This characterized the formation of the MCS nonlinear event of 15 January 1993 (Fig. 3c). The convective region was embedded in a broad stratiform precipitation region, which formed and expanded where previously collocated convective cells had collapsed and decayed. The stratiform rain region persisted following the decay of the convective cells and slowly dissipated with time.

Finally, when convection formed a well-defined line of cells at least 100 km in length, the event was termed ''MCS linear.'' These systems typically consisted of either propagating squall lines or slow-moving convective bands, with associated stratiform precipitation. It was common for squall lines to form behind or enter into the wake of stratiform precipitation from a preceding line. The example in Fig. 3d (25 December 1992) shows the last of a series of four large squall lines that occurred in succession over the previous 18 h. The line shown in Fig. 3d propagated to the northeast through a broad stratiform region associated with the preceding three lines. For that reason, multiple lines or new lines occurring within preexisting stratiform precipitation were considered part of the same event. Detailed case studies of TOGA COARE convection (e.g., Jorgensen et al. 1997) have discussed the evolution and interaction between multiple lines; however, the focus here was only on the presence or absence of a general class of convective organization.

All convection present within a particular event period was characterized by the organization of the spatially largest region of convection. For example, isolated cells surrounding a squall line were included as an MCS linear event. In practice, persistent coexistence of two or more different organization levels greater than sub-MCS nonlinear did not occur within the radar domain.

b. Convective–stratiform partitioning and rainfall estimation

Previous case studies of MCSs have discussed dynamical and microphysical distinctions between convective and stratiform precipitation, resulting in distinct vertical profiles of heating associated with both precipitation types (cf., section 1). The relative amount of convective versus stratiform rain produced by a precipitating system thus provides insight as to the dominant microphysical processes that produce the precipitation in MCSs, and how the resultant latent heating of the atmosphere is distributed vertically (Houze 1989). It is therefore important to estimate the relative amount of convective and stratiform rain associated with each event.

Tokay and Short (1996) analyzed raindrop size distribution data from surface disdrometers on Kapingamarangi Atoll during COARE. They found distinct size spectra, attributable to unique drop size distributions in convective and stratiform rain. This observation led them to derive separate reflectivity-rainfall rate (Z-R) relations for each rain type:

$$Z = 139R^{1.43} \quad \text{(convective)}, \tag{1}$$

$$Z = 367R^{1.30} \quad \text{(stratiform)}. \tag{2}$$

These relations illustrate the conclusion of Tokay and Short (1996) that for COARE, a stratiform raindrop population produced roughly half the rainfall rate compared to that of convective regions for a given reflectivity value. This was because the presence of a few very large drops (formed from the melting of large aggregates) in the stratiform drop spectra increases the radar reflectivity much more than it increases the rain volume.[1] It was therefore necessary to distinguish between convective and stratiform rain when making a quantitative estimate of rainfall rates in the COARE region.

The ideal approach to distinguishing between convective and stratiform regions is to identify by direct measurements areas where ice particles fall relative to the surrounding air (Houze 1993; Willis et al. 1995). Unfortunately, measurements of vertical motion coincident with particle fall speeds are rare, and are not generally available for COARE systems sampled by the ship radars.

Accordingly, indirect methods for identifying regions where particle fall speeds exceed the vertical air speed had to be used. These techniques typically involved identifying convective rain regions rather than stratiform rain regions, because the vertical resolution of the Cartesian reflectivity data was generally too coarse to resolve the stratiform radar bright band. The most common approach was to examine spatial gradients of a low-level map of radar reflectivity to isolate regions of more intense, horizontally variable precipitation indicative of convective rain from regions of horizontally uniform precipitation associated with stratiform rain (Churchill and Houze 1984; Steiner et al. 1995). This

[1] Drop volume is proportional to the third power of the drop radius, and radar reflectivity is proportional to the sixth power of the drop radius.

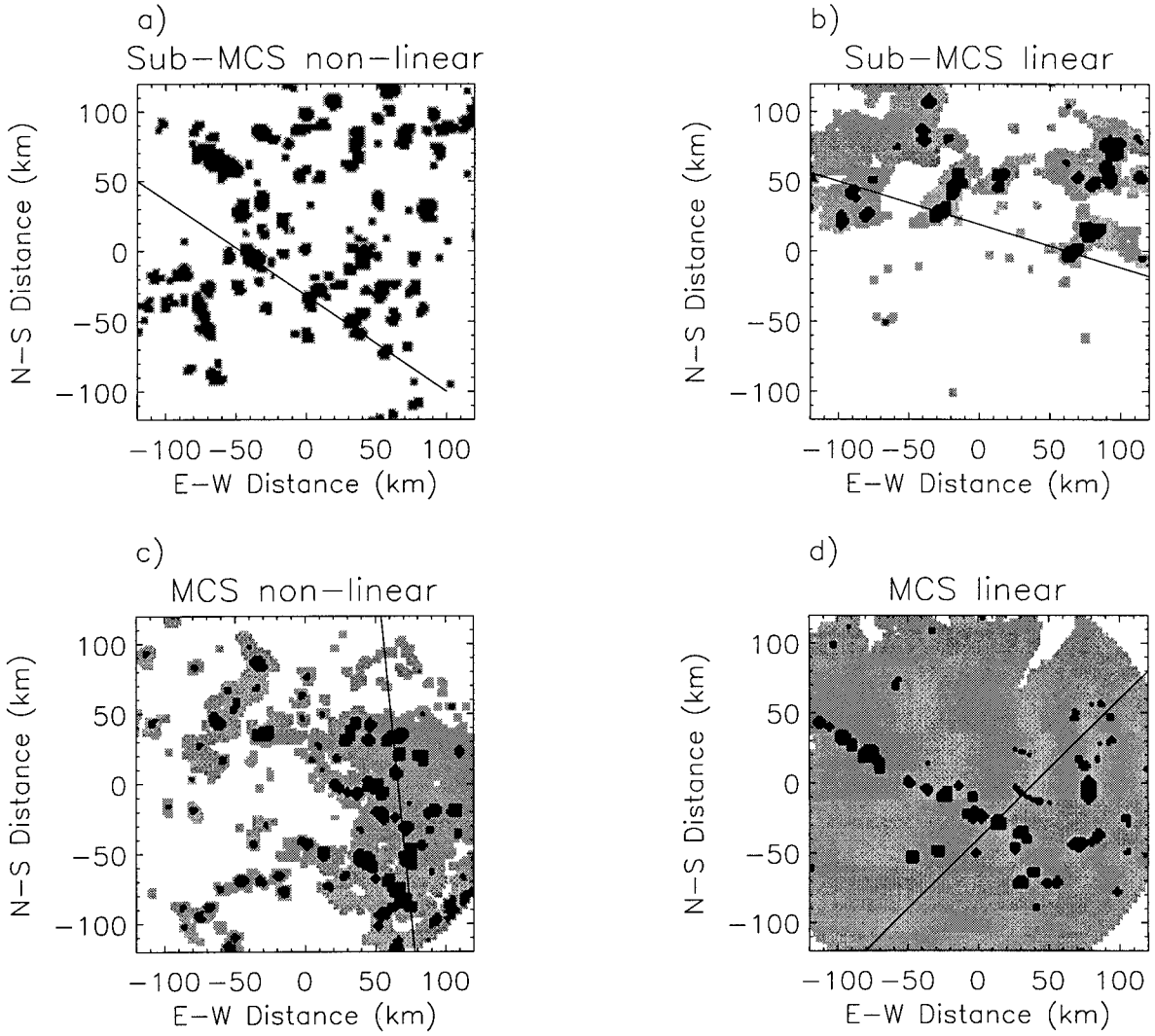

FIG. 4. Maps of the convective–stratiform separation at a height of 2 km corresponding to the reflectivity maps shown in Fig. 3 for (a) a sub-MCS nonlinear event at 0721 UTC 2 December 1992, (b) a sub-MCS linear event at 1002 UTC 27 December 1992, (c) an MCS nonlinear event at 1802 UTC 15 January 1993, and (d) an MCS linear event at 0331 UTC 25 December 1992. Convective regions are shown in black, stratiform regions in gray, reflectivity-free zones in white. Distinct black regions denote convective features, as discussed in the text.

technique involved an examination of the low-level horizontal radar reflectivity field for two criteria related to the spatial uniformity of rainfall that indicate the center of a convective area: *intensity* and *peakedness*. The intensity criterion for convective rain was satisfied wherever reflectivity exceeds 40 dB*Z*, accounting for observations that stratiform reflectivities did not generally exceed this value 2 km above the surface (Steiner et al. 1995). In addition, any other local maximum may be considered convective if it stood out from the local background by about a factor of two in rainfall rate, in the following way. If a local reflectivity maximum less than 40 dB*Z* exceeded the mean reflectivity in an 11-km radius circle surrounding the point by 4.5 dB (roughly a factor of 2 rainfall rate difference), it was considered convective. This was termed the ''peakedness'' criterion by Steiner et al. (1995). Once a point reflectivity value was denoted as convective, a circular ''convective cell'' with a radius that increased with the mean background reflectivity was placed around the point. The radius of this circular ''cell'' varied between 1 and 5 km. All other reflectivity values were considered stratiform. The method used herein followed that of Steiner et al. (1995), except for a difference in how the peakedness criterion was applied (see appendix A).

Shown in Fig. 4d is the convective–stratiform separation for the MCS linear example of Fig. 3d. The algorithm identified convective elements associated with the decaying squall line surrounded by a large stratiform region. The line-normal cross section showed the strong leading edge cell, the trailing stratiform reflectivity maximum just below the melting level (~5 km), and a nar-

row band of developing convection 30 km in front of the main line. Small groups of convective cells are embedded within the stratiform region, corresponding to local maxima in the reflectivity field.

The convective–stratiform map corresponding to the MCS nonlinear example of Fig. 3c is given in Fig. 4c. The map indicated widespread groups of convective cells, embedded within stratiform rain. The cross section of Fig. 3c suggested that much of the embedded convection was deep. In contrast, vertically developed convection associated with the sub-MCS linear example (Fig. 3b) was limited to the leading edge of each small line (convective–stratiform map shown in Fig. 4b). However, Figs. 4b and 4c revealed a limitation in the convective–stratiform separation technique for situations where weak isolated cells coexisted with organized convection. Many weak isolated convective cells did not meet either the intensity or peakedness criteria and were therefore not indicated by the algorithm as convective. This became especially problematic for sub-MCS nonlinear events where isolated cells dominated the reflectivity pattern. Tuning the algorithm to favor the performance with isolated convection came at the expense of results for organized convection. The compromise used herein was to assign all sub-MCS nonlinear echo as convective (Fig. 4a), while retaining the current algorithm for all other situations. The effect of this compromise on the rainfall totals was small ($<2\%$).

The appropriate Z–R relation was applied to convective and stratiform reflectivity values in order to calculate rainfall rates. These rainfall rates were then corrected for attenuation of the beam by intervening precipitation, which can be significant at C-band, following Patterson et al. (1979). The attenuation correction was therefore dependent on the convective–stratiform rainfall partition, since the correction was applied to the rainfall rate fields. This correction increased the mean 80-day total rainfall rate by about 10%. No other correction was applied to the reflectivity values (e.g., removal of anomalous propagation, manual editing of sea clutter) because of the large number of data volumes used. For these reasons, relative rainfall amounts between modes of convective organization were given more emphasis than absolute rainfall amounts.

c. Convective feature identification

Once the convective–stratiform status of points on each horizontal reflectivity map at 2 km height was determined, convective grid points were grouped into ''convective features.'' A convective feature was defined as a group of adjacent grid points (including diagonally adjacent), which have been labeled as convective by the convective–stratiform separation algorithm for each horizontal map of reflectivity at a height of 2 km. As such, a single convective feature may contain one or more individual convective cells. Each convective feature was isolated from other features by stratiform grid points or reflectivity-free regions. Examples of convective features can be seen as the distinct black regions in the convective–stratiform separation maps (Fig. 4). For each reflectivity volume, all convective features were uniquely identified, and the maximum height and rainfall rate calculated for each feature. The convective feature height was defined to be the highest vertical extent of echo anywhere within the feature. In this way, the variation with scale and morphology in the size distribution of merged convective elements could be studied. Convective feature statistics were thus related to the temporal integration of the instantaneous echo population.

4. Results

a. Rainfall and zonal wind time series

Shown in Figs. 5a–c are time series of the rainfall rate averaged over the entire radar domain for each cruise, color coded to indicate the mode of convective organization present. Rainfall was nearly continuous, punctuated by local maxima ranging from 5 mm d^{-1} to 50 mm d^{-1}. These maxima corresponded to the formation and decay of precipitation events within the radar sample area, and to the propagation of events across the sample area. To place the rainfall time series in the context of the mean flow, the corresponding time–height series of the daily mean tropospheric zonal wind from the sounding data discussed in section 2 is given in Figs. 6a–c. The most conspicuous feature was the strong westerly wind burst centered at a height of 4–8 km in late December and early January, in the wake of the convectively active phase of the intraseasonal oscillation (Lin and Johnson 1996a). A weaker westerly burst was present during the beginning of February, followed by sustained weaker westerlies for the remainder of that month. The month of November was characterized by relatively weak low-level winds, which oscillated between easterly and westerly. Between 13 and 24 November, this oscillation displayed a period of 4–5 days, and had a phase consistent with the westward propagating near-equatorial wind oscillations present at that time (Numaguti et al. 1995). The only sustained period of easterly winds in the lower troposphere occurred during mid-January, with upper-tropospheric westerlies replacing the more typical easterlies.

Rainfall rate maxima above about 15 mm d^{-1} were consistently associated with MCS-scale events. The duration of these MCS rainfall periods (comprising one or more events) varied from 6 h to about 1.5 days. MCS-scale events occurred in all wind regimes, but were most common in late December to early January and in February associated with strong westerly winds. However, at the time of the two low-level westerly wind burst maxima (30 December–1 January and 2–5 February), no MCS-scale events were present. In fact, these periods were characterized by almost no rainfall whatsoever.

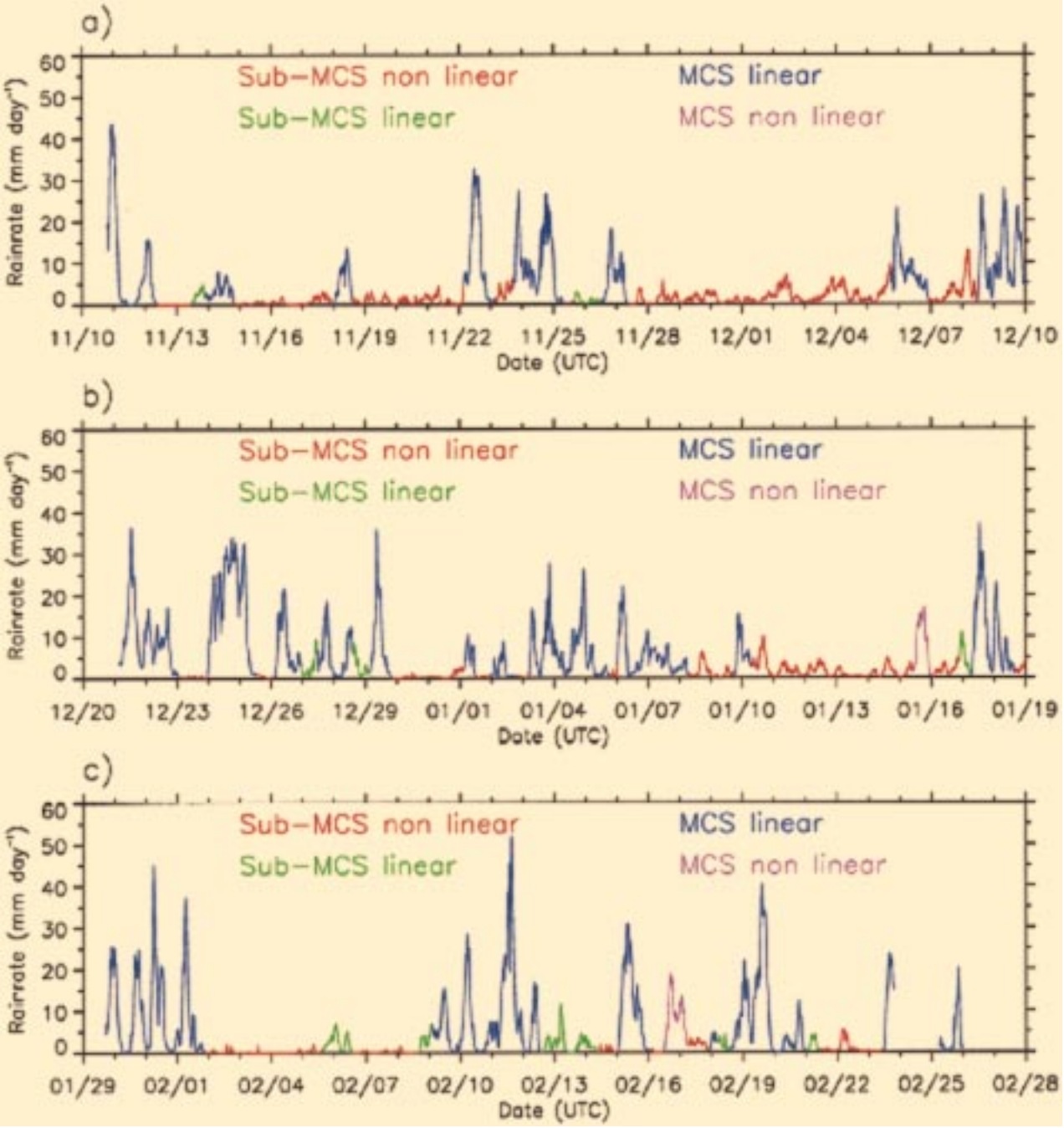

FIG. 5. Time series of rain rate (mm day^{-1}) for (a) cruise 1, (b) cruise 2, and (c) cruise 3. The category of organization present is indicated with a color-coded rainfall trace as follows: sub-MCS nonlinear (red), sub-MCS linear (green), MCS nonlinear (purple), and MCS linear (blue).

The heaviest (MCS scale) rainfall preceded the westerly wind maxima, which is consistent with studies by Lau et al. (1989) and Lin and Johnson (1996a) of convection in the equatorial western Pacific Ocean region. It is also worth noting that sustained MCS-scale convection also followed the westerly bursts, occurring two to five days after the wind maxima. The unique period between 16 and 19 January, where low-level easterlies and upper-level westerlies occurred, was dominated by MCS linear events. The propagation direction of squall lines and groups of convective cells was generally in the direction of the mean wind near 800 mb. An analysis of system motion will be presented in a separate study.

There were several multiday periods during which

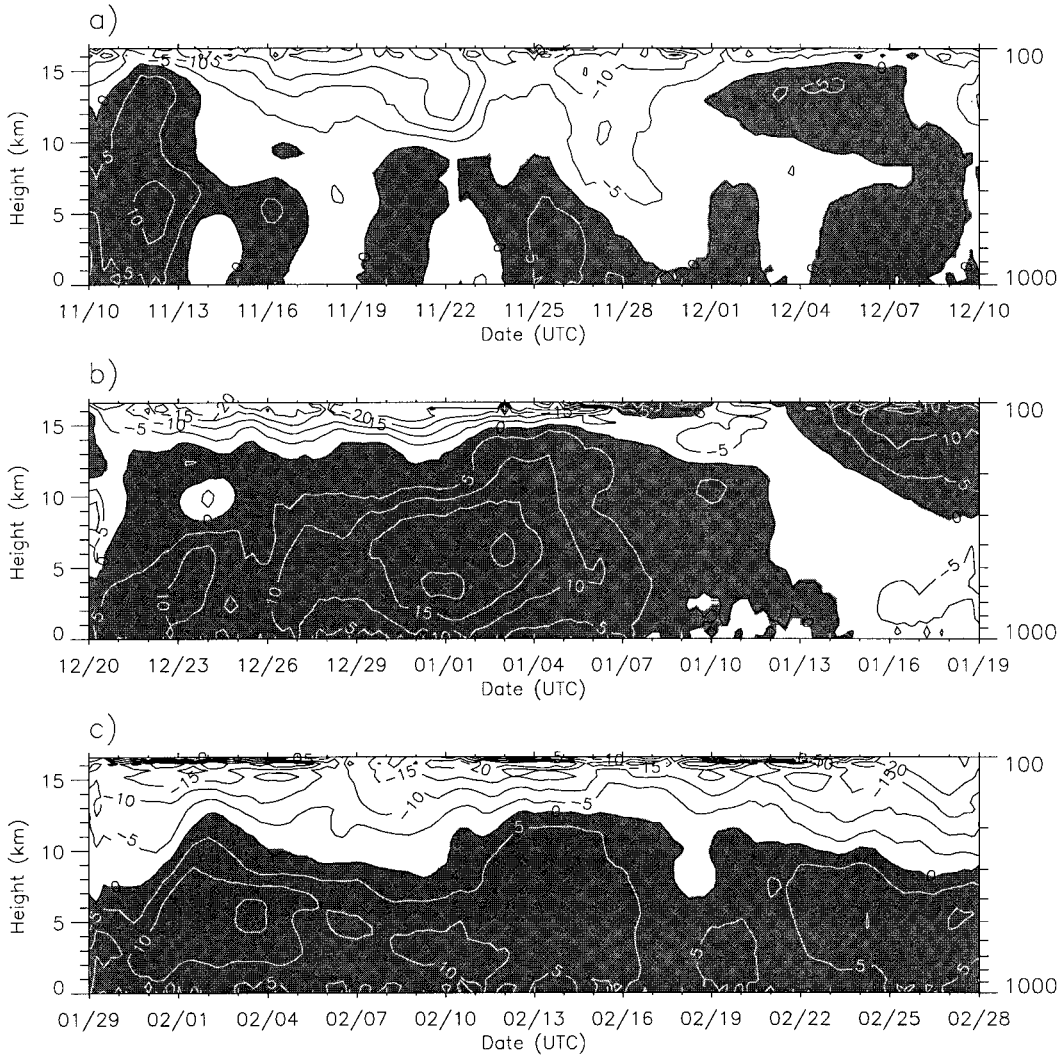

FIG. 6. Time series of the vertical profile of zonal wind (m s^{-1}) for (a) cruise 1, (b) cruise 2, and (c) cruise 3 in the vicinity of the MIT radar, from sounding data. The right vertical axis scale shows pressure (mb) in increments of 100 mb. Positive values (shaded) are westerly. Contour interval is 5 m s^{-1}.

sub-MCS nonlinear events produced all of the rainfall. The longest periods occurred from 28 November to 5 December and from 10 to 15 January. These time intervals were characterized by light winds near the surface. However, multiday periods of sub-MCS nonlinear organization were not limited to periods of light wind near the surface, as discussed above.

b. Eighty-day mean rainfall statistics

The 80-day mean rainfall rate and convective rainfall fraction from the MIT radar data were 4.5 mm d^{-1} and 72%, respectively. The rainfall rate was close to the value of 4.8 mm d^{-1} obtained by Short et al. (1997) for the combined TOGA and MIT radar datasets. The convective rain fraction fell within the range of those reported in previous climatological studies of tropical rainfall from radar and rain gauge data. Cheng and Houze (1979) estimated a convective rainfall fraction of 60% for GATE convection from all scales of radar echo. Rosenfeld et al. (1995) estimated a convective rain fraction of 78% from rain gauge data for maritime ITCZ convection. They suggested that previous radar case studies underestimated the convective rain fraction by not accounting for the distinct drop size distributions (and thus reflectivity–rainfall relations) in convective versus stratiform rain (e.g., Waldvogel 1974; Tokay and Short 1996). Steiner et al. (1995) reported a range of convective rainfall fractions between 59% and 66% for a one month sample of radar data in the vicinity of Darwin, Australia.

The 80-day total rainfall production and event occurrence frequency partitioned by scale and morphology are given in Fig. 7. Sub-MCS nonlinear (isolated cells)

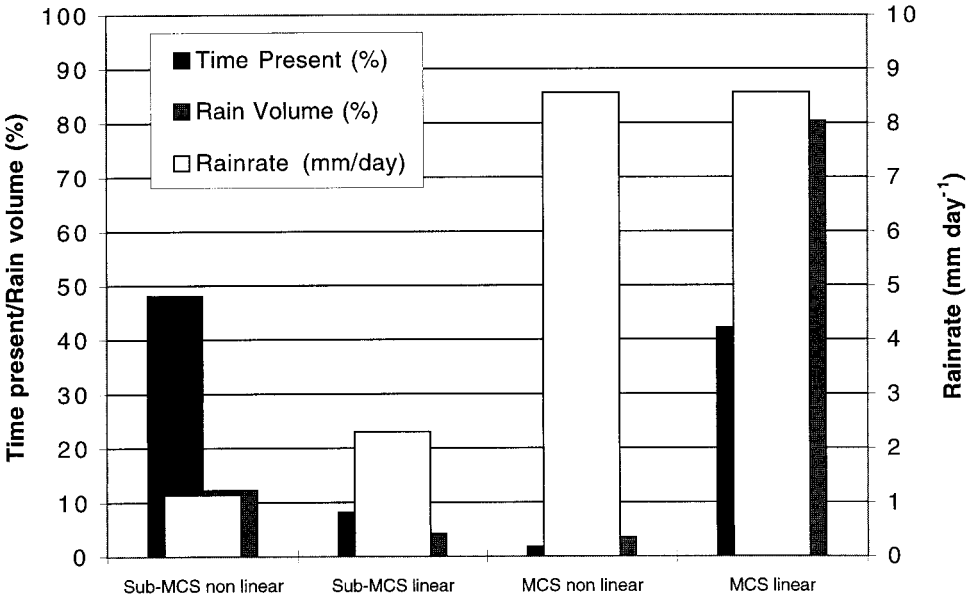

FIG. 7. The time present (black), rain volume (gray), and mean areally averaged rainfall rate (white, mm day^{-1}) for each event type for all three cruises combined. Time present and rain volume are expressed as fractions of the three-cruise totals.

and MCS linear (large squall lines) were the most frequently observed modes of organization. Both these event types were about equally as common, with one or the other present just over 90% of the time. The dominant rain producing mode was MCS linear, contributing 80% of the total rain volume. Although sub-MCS scale nonlinear rainfall was present 48% of the time, the rain volume associated with these events comprised 12% of the total 80-day rain volume. As a comparison, Simpson et al. (1993) found that, for island convection in the southern maritime continent region near Darwin, Australia, less than 10% of the observed precipitation was associated with isolated convective cells, which is consistent with the present result. In contrast, sub-MCS linear and MCS nonlinear events are comparatively rare, with 8% and 3% occurrence, respectively. The mean areally averaged rainfall rates of MCS events (8.5 mm d^{-1}) were much higher than those on the sub-MCS scale, associated with large areal coverage of precipitation.

The mean convective rainfall fraction was calculated for each event type, breaking down as follows: sub-MCS nonlinear, 100%; sub-MCS linear, 80%; MCS nonlinear, 83%; MCS linear, 66%. Large squall line events (MCS linear) had the lowest mean convective fraction, and was in good agreement with several case studies of individual tropical squall lines over the entire system lifetime (Houze 1977, 60%; Gamache and Houze 1983, 51%; Houze and Rappaport 1984, 58%). However, the comparison of the MCS linear convective fraction to these case studies must be done with caution, since the present result represents a combination of many events over different portions of their life cycle. Previous studies of tropical squall lines over a portion of the system's lifetime produced a broader range of results (Leary 1984, 70%; Zipser et al. 1981, 45%–50%), within which the current estimate of the MCS linear event convective rain fraction falls.

c. Convective feature height/rain distributions

The rainfall contribution from convective features of various heights, by scale, morphology, and for all events combined, is shown in Fig. 8a. The distribution for all events showed two distinct maxima, with a primary rainfall maximum at the 14–15-km feature height bin and a secondary maximum at 9–10 km. This result is generally consistent with an analysis of a group of mesoscale precipitation features (Leary 1984) over a 24-h period during GATE. However, the secondary maximum in rainfall from convective features of 9–10-km height was not seen during GATE.

These rainfall–convective feature height distributions differed significantly when partitioned by the four categories of horizontal organization. The shape of the rainfall distribution from MCS linear events was similar to the total but with more rain associated with deeper features and less in shallower features. For MCS nonlinear events, these two maxima were much more pronounced, though the small sample size of that event type precluded ascribing much significance to the sharpness of these maxima. In contrast, the distribution of sub-MCS-scale nonlinear events was clearly centered at 8–9 km. Sub-MCS-scale linear events showed a slightly shal-

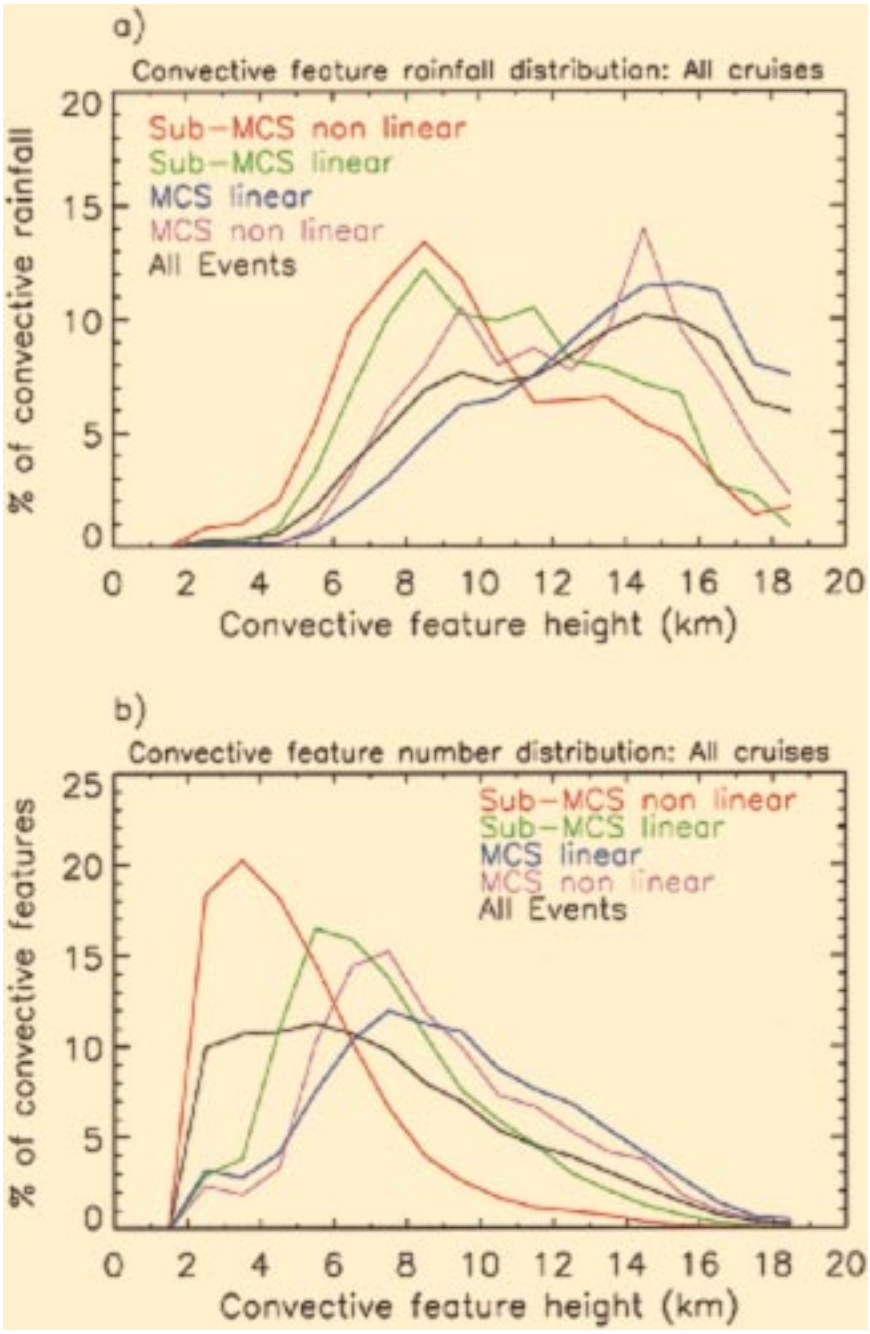

FIG. 8. Histograms of (a) the fraction of rainfall (convective only) produced by convective features, (b) the convective feature frequency distribution for convective features, between 1 and 19 km in height (1 km bins), for each event type and for all events combined. Each histogram represents the fraction of convective rain produced by that event type. Color coding of each event type is as in Fig. 5.

lower peak at the same height level, with more rainfall shifted to deeper convective features. The contribution of sub-MCS-scale rain to the lower ''all event'' peak was not large, since 80% of total rainfall occurs with MCS-scale events (cf. Fig. 7). Above the 14–15-km height bin, the all event distribution was dominated by MCS-scale features. Thus the bimodal structure for all events combined appeared to be related to distinct convective feature height populations associated with sub-MCS-scale and MCS-scale events.

In order to understand this distribution further, the number distribution of convective features over the

spectrum of observed feature heights is shown in Fig. 8b. The all event number distribution indicated that more than 60% of all convective features were between 2 km and 8 km in height, with a local maximum at 5–6 km. Above 8 km, the height frequency decreased linearly to 18–19 km height. A comparison with Fig. 8a showed that the rainfall from convective features higher than 14–15 km (40% of the convective rain) for all events was associated with less than 5% of all features. The frequency distribution for GATE radar echoes (Houze and Cheng 1977) was quite similar to the all event distribution. The COARE all event distribution appeared to be composed of a superposition of distinct distributions associated with each mode of organization. Furthermore, as the convective organization increased (e.g., sub-MCS nonlinear to MCS linear), the distribution transitioned from an exponential to a linear decrease in the number of features with height. The height peak in the distributions also increased and broadened with an increase in organization. The contrast was greatest between the two most common modes: MCS linear and sub-MCS nonlinear. The sub-MCS nonlinear distribution had a sharp peak at 3–4 km, which decreased exponentially above that height. Therefore, the absence of a maximum of rainfall from deep convective features for sub-MCS-scale nonlinear events was due to the rarity of deep convective features from those events. In contrast, the distribution for MCS linear events was more Gaussian, with the mode at 7–8 km.

The rainfall distribution shown in Fig. 8a provided a lower limit estimate of rainfall produced by isolated shallow convection where only collision and coalescence processes were active (''warm rain'' clouds). Since the 0°C level was generally located near 5.5 km (Johnson et al. 1996), convective features with echo top height at or below this level were likely dominated by warm rain processes. For all events combined, nearly 3% of the total rainfall was associated with echo tops below 5.5 km. For sub-MCS-scale nonlinear events, this value increased to 9%. However, these are lower limit estimates, since warm rain processes were most likely active below the 0°C level even in deep convection.

5. Summary

An 80-day sample of convection was examined using shipboard radar reflectivity data during TOGA COARE, between November 1992 and February 1993. This unprecedented view of oceanic convection over the warm pool region of the western Pacific Ocean allowed for the study of rainfall associated with a broad spectrum of convective organization. The main purpose of this study was to give an overview of and present statistics on the modes of convective organization present, from the perspective of an Eulerian sample of radar reflectivity. This provides a context in which to place detailed case studies of individual events.

A simple system of classifying convective organization was developed based on the scale and morphology attained during convective events. This system accounted for the evolution of individual events constrained by the timescale of advection (6–12 h) across the radar domain. The scale of horizontal organization was defined with respect to the minimum dimension of an MCS, and morphology in terms of the presence or absence of linear organization. Reflectivity fields were partitioned into convective and stratiform components. This allowed the convective versus stratiform rainfall fractions and the rainfall and depth of convective reflectivity features to be studied, in the context of horizontal organization.

TABLE 1. Summary of the fraction of time present, rain volume fraction, and convective rainfall fraction for each of the four modes of convective organization.

	Fraction of time present	Rain volume fraction	Convective rain fraction
Sub-MCS nonlinear	48%	12%	100%
Sub-MCS linear	8%	4%	80%
MCS nonlinear	2%	4%	83%
MCS linear	42%	80%	66%

It was found that just over four-fifths of the total rainfall was associated with convective organization on the MCS scale. Almost all MCS-scale convection (95%) occurred as squall lines or convective bands. The mean convective rainfall fraction of MCS linear events (66%) was within the range of many previous case studies of tropical squall line systems. These events were present 43% of the time and were more common prior to low-level westerly wind burst maxima. However, MCS-scale convection was observed in all wind regimes during COARE.

The most common mode of organization were fields of isolated convective cells (sub-MCS nonlinear), present 48% of the time. These events were an important contributor to the total rainfall, accounting for 12% of the total rain. Two extended periods (6–8 days each) of sub-MCS nonlinear organization coincided with light near-surface winds. However, these events also dominated the period during the late December and early February low-level westerly wind burst maxima. These observations are suggestive of an optimal shear regime allowing organized convection (Rotunno et al. 1988). Lines of convection on the sub-MCS scale were uncommon, while MCS nonlinear events were quite rare. The reason for this appeared to be that when convection began to organize upscale, short lines often merged to long lines, and MCS-scale clusters of cells generally transitioned to linear organization. A summary of the main rainfall and occurrence frequency statistics for each mode of organization are given in Table 1.

The distribution of total rainfall by convective feature height resulted from the superposition of distinct distributions from each mode of organization. Most convective rainfall for all event types combined was as-

sociated with deep (14–15-km height) convective reflectivity features. A secondary maximum of rainfall occurred for features of 8–10 km in height. In contrast, the distributions for sub-MCS nonlinear events were quite distinct, with a rainfall peak from convective features of 8–9 km in height, and a frequency peak at 3–4 km in height. A possible explanation for the midlevel maximum on both scales may lie in the presence of a ubiquitous dry stable layer near the 0°C level (~5.5 km) as discussed in Johnson et al. (1996). This layer may attenuate the upward momentum of buoyant parcels ascending from the boundary layer and entrain dry air into the cloud, limiting the vertical development of convection to a few kilometers above the stable layer. On the sub-MCS scale, the inversion may attenuate most convection, leading to a sharp midlevel peak. On the MCS scale, convection may be of sufficient strength for more cells to penetrate to the tropopause, resulting in a smaller midlevel peak and a large upper-level peak from a relatively few heavy raining convective features. This is consistent with the sustained forced ascent at the leading edge of squall lines, maintaining deep, heavy raining convection.

The common occurrence, significant rainfall production, and distinct cloud populations of isolated cell periods compared to large squall line systems suggest that attention should be given to both modes of convective organization. The occurrence of long periods of MCS-scale convection appeared to be associated with strong IFA-mean tropospheric heating discussed in Lin and Johnson (1996b). However, since isolated convection had a distinct vertical structure and produced nonnegligible rainfall relative to MCS-scale systems, the role of prolonged, extensive isolated convection on the large-scale heat budget should be examined. Detailed analyses must be performed on individual cases for systems of both scales and their environments to quantify these effects.

Acknowledgments. Prof. Richard Johnson, Dr. Xin Lin, and Mr. Paul Ciesielski of Colorado State University are gratefully acknowledged for providing the sounding data. This study would not have been possible without the efforts of the many scientists, engineers, and managers who made contributions prior to and during the COARE IOP to make the shipboard radar program a success. Discussions with Shuyi Chen, Rob Cifelli, Charlotte DeMott, Richard Johnson, Brian Mapes, Rosana Nieto Ferreira, Walt Petersen, and Wayne Schubert influenced the design of this work. We thank the reviewers for particularly constructive comments. One of us (TMR) acknowledges the support of a National Research Council Associateship at the NASA/Goddard Space Flight Center during the completion of this work. This research was funded by the National Oceanic and Atmospheric Administration TOGA COARE Grant NA90RAH00077 and Colorado State University.

APPENDIX

Convective–Stratiform Partitioning Method

Steiner et al. (1995) discuss the need to ''tune'' the peakedness criterion in their convective–stratiform partitioning technique for a particular geographic region and radar. The tuning involves modulating the threshold value that the point in question must exceed the background reflectivity area by to be considered convective with the value of the background area (the ''tuning curve,'' Fig. 7 of Steiner et al. 1995). However, tuning the algorithm ultimately relied on a subjective evaluation of the algorithm's performance. To minimize the subjectivity inherent in the technique, the effect of the tuning on the 80-day rainfall, convective fractions, and rainfall distribution by height was examined. A comparison was made of these parameters using the tuning curve for Darwin (Steiner et al. 1995) versus using a constant threshold value (4.5 dB; Steiner and Houze 1993) for the peakedness criterion. The difference in both the mean rainfall rate and the convective rain fraction is about 3%–4% lower for the constant threshold case. This difference was smaller than errors introduced by subjective (visual inspection) determination of the algorithm's performance. Such a subjective analysis would be required to tune the algorithm. Moreover, the TOGA C-band radar used in Darwin has nearly identical specifications as the MIT radar. Therefore, the tuning procedure was not performed for the present study.

REFERENCES

Biggerstaff, M. I., and R. A. Houze, 1991: Kinematic and precipitation structure of the 10–11 June 1985 squall line. *Mon. Wea. Rev.,* **119,** 3034–3065.

Bluestein, H. B., and M. H. Jain, 1985: Formation of mesoscale lines of precipitation: Severe squall lines in Oklahoma during the spring. *J. Atmos. Sci.,* **42,** 1711–1732.

Cheng, C., and R. A. Houze, 1979: The distribution of convective and mesoscale precipitation in GATE radar echo patterns. *Mon. Wea. Rev.,* **107,** 1370–1381.

Churchill, D. D., and R. A. Houze Jr., 1984: Development and structure of winter monsoon cloud clusters on 10 December 1978. *J. Atmos. Sci.,* **41,** 933–960.

Cotton, W. R., and R. Anthes, 1991: *Cloud and Storm Dynamics.* Academic Press, 883 pp.

Gamache, J. F., and R. A. Houze, 1983: Water budget of a mesoscale convective system in the Tropics. *J. Atmos. Sci.,* **40,** 1835–1850.

Greco, S., and Coauthors, 1990: Rainfall and surface kinematic conditions over central Amazonia during ABLE 2B. *J. Geophys. Res.,* **95,** 17 001–17 014.

Houze, R. A., 1977: Structure and dynamics of a tropical squall-line system. *Mon. Wea. Rev.,* **105,** 1540–1567.

——, 1982: Cloud clusters and large-scale vertical motions in the Tropics. *J. Meteor. Soc. Japan,* **60,** 396–410.

——, 1989: Observed structure of mesoscale convective systems and implications for large scale heating. *Quart. J. Roy. Meteor. Soc.,* **115,** 425–461.

——, 1993: *Cloud Dynamics.* Academic Press, 573 pp.

——, and C. Cheng, 1977: Radar characteristics of tropical convection observed during GATE: Mean properties and trends over the summer season. *Mon. Wea. Rev.,* **105,** 964–980.

——, and A. K. Betts, 1981: Convection in GATE. *Rev. Geophys. Space Phys.,* **19,** 541–576.

——, and E. N. Rappaport, 1984: Air motions and precipitation structure of an early summer squall line over the eastern tropical Atlantic. *J. Atmos. Sci.,* **41,** 553–574.

——, B. F. Smull, and P. Dodge, 1990: Mesoscale organization of springtime rainstorms in Oklahoma. *Mon. Wea. Rev.,* **118,** 613–654.

Johnson, R. H., 1984: Partitioning tropical heat and moisture budgets into cumulus and mesoscale components: Implications for cumulus parameterization. *Mon. Wea. Rev.,* **112,** 1590–1601.

——, P. E. Ciesielski, and K. A. Hart, 1996: Tropical inversions near the 0°C level. *J. Atmos. Sci.,* **53,** 1838–1855.

Jorgensen, D. P., M. A. LeMone, and S. B. Trier, 1997: Structure and evolution of the 22 February 1993 TOGA COARE squall line: Aircraft observations of precipitation, circulation, and surface energy fluxes. *J. Atmos. Sci.,* **54,** 1961–1985.

Keenan, T. D., and R. E. Carbone, 1992: A preliminary morphology of precipitation systems in tropical northern Australia. *Quart. J. Roy. Meteor. Soc.,* **118,** 283–326.

Lau, K. M., L. Peng, C. H. Sui, and T. Nakazawa, 1989: Dynamics of super cloud clusters, westerly wind bursts, 30–60 day oscillations and ENSO: A unified view. *J. Meteor. Soc. Japan,* **67,** 205–219.

Leary, C. A., 1984: Precipitation structure of the cloud clusters in a tropical easterly wave. *Mon. Wea. Rev.,* **112,** 313–325.

——, and R. A. Houze, 1979: The structure and evolution of convection in a tropical cloud cluster. *J. Atmos. Sci.,* **36,** 437–457.

LeMone, M. A., 1983: Momentum transport by a line of cumulonimbus. *J. Atmos. Sci.,* **40,** 1815–1834.

——, G. M. Barnes, and E. J. Zipser, 1984: Momentum flux by lines of cumulonimbus over the tropical ocean. *J. Atmos. Sci.,* **41,** 1914–1932.

Lin, X., and R. H. Johnson, 1996a: Kinematic and thermodynamic characteristics of the flow over the western Pacific warm pool during TOGA COARE. *J. Atmos. Sci.,* **53,** 695–715.

——, and ——, 1996b: Heating, moistening and rainfall analysis over the western Pacific warm pool during TOGA COARE. *J. Atmos. Sci.,* **53,** 3367–3383.

Loehrer, S. M., and R. H. Johnson, 1995: Surface pressure and precipitation life cycle characteristics of PRE-STORM mesoscale convective systems. *Mon. Wea. Rev.,* **123,** 600–621.

Nakazawa, T., 1988: Tropical super clusters within intraseasonal variations over the western Pacific. *J. Meteor. Soc. Japan,* **66,** 823–839.

Numaguti, A., R. Oki, K. Nakamura, K. Tsuboki, N. Misawa, T. Asai, and Y-M. Kodama, 1995: 4–5 day-period variation and low-level dry air observed in the equatorial western Pacific during the TOGA-COARE IOP. *J. Meteor. Soc. Japan,* **73,** 267–290.

Orlanski, I., 1975: A rational subdivision of scales for atmospheric processes. *Bull. Amer. Meteor. Soc.,* **56,** 527–530.

Patterson, V. L., M. D. Hudlow, P. J. Pytlowany, F. P. Richards, and J. D. Hoff, 1979: GATE radar rainfall processing system. NOAA Tech. Memo. EDIS 26, NOAA Washington, DC, 34 pp.

Riehl, H., and J. S. Malkus, 1958: On the heat balance in the equatorial trough zone. *Geophysica,* **6,** 503–538.

Rosenfeld, D., E. Amitai, and D. B. Wolff, 1995: Classification of rain regimes by the three-dimensional properties of reflectivity fields. *J. Appl. Meteor.,* **34,** 198–211.

Rotunno, R., J. B. Klemp, and M. L. Weisman, 1988: A theory for strong, long-lived squall lines. *J. Atmos. Sci.,* **45,** 463–485.

Rutledge, S. A., and R. A. Houze, 1987: A diagnostic modeling study of the trailing stratiform region of a midlatitude squall line. *J. Atmos. Sci.,* **44,** 2640–2656.

——, and Coauthors, 1993: The shipboard deployment of the MIT C-band radar during TOGA COARE. Preprints, *26th Int. Conf. on Radar Meteorology,* Norman, OK, Amer. Meteor. Soc., 371–373.

Schmidt, J. M., and W. R. Cotton, 1989: A high plains squall line associated with severe surface winds. *J. Atmos. Sci.,* **46,** 281–301.

Short, D. A., P. A. Kucera, B. S. Ferrier, J. C. Gerlach, S. A. Rutledge, and O. W. Thiele, 1997: Shipboard radar rainfall patterns within the TOGA COARE IFA. *Bull. Amer. Meteor. Soc.,* **78,** 2817–2836.

Simpson, J., T. D. Keenan, B. Ferrier, R. H. Simpson, and G. J. Holland, 1993: Cumulus mergers in the maritime continent region. *Meteor. Atmos. Phys.,* **51,** 73–99.

Steiner, M., and R. A. Houze, 1993: Three-dimensional validation at TRMM ground truth sites: Some early results from Darwin, Australia. Preprints, *26th Int. Conf. on Radar Meteorology,* Norman, OK, Amer. Meteor. Soc., 417–420.

——, ——, and S. E. Yuter, 1995: Climatological characteristics of three-dimensional storm structure from operational radar and raingauge data. *J. Appl. Meteor.,* **34,** 1978–2007.

Tokay, A., and D. A. Short, 1996: Evidence from tropical raindrop spectra of the origin of rain from stratiform versus convective clouds. *J. Appl. Meteor.,* **35,** 355–371.

Waldvogel, A., 1974: The N_0 jump of raindrop spectra. *J. Atmos. Sci.,* **31,** 1068–1078.

Webster, P. J., and R. Lukas, 1992: TOGA COARE: The coupled ocean-atmosphere response experiment. *Bull. Amer. Meteor. Soc.,* **73,** 1377–1416.

Willis, P., R. A. Black, F. D. Marks, and D. Baumgardner, 1995. Airborne rain drop size distributions in TOGA COARE. Preprints, *21st Conf. on Hurricanes and Tropical Meteorology,* Miami, FL, Amer. Meteor. Soc., 431–433.

Zipser, E. J., 1977: Mesoscale and convective-scale downdrafts as distinct components of squall-line circulation. *Mon. Wea. Rev.,* **105,** 1568–1589.

——, R. J. Meitin, and M. A. LeMone, 1981. Mesoscale motion fields associated with a slowly moving GATE convective band. *J. Atmos. Sci.,* **38,** 1725–1750.